THE ASTROPHYSICAL JOURNAL, 365:66–85, 1990 December 10

A DEEP ABELL CLUSTER REDSHIFT SURVEY[1]

J. P. HUCHRA,[2] J. P. HENRY,[3] M. POSTMAN,[4] AND M. J. GELLER[2]

Received 1989 August 29; accepted 1990 June 12

ABSTRACT

We have measured redshifts for a complete sample of 145 Abell clusters of galaxies. The sample covers a 561 square degree region at high Galactic latitude. The median redshift of the clusters in the sample is 0.16. For $R \geq 1$ clusters the correlation length is $r_0 = 21h^{-1}$ Mpc. The amplitude of the correlation function is a factor of 1.4 less than that obtained by Bahcall and Soneira, but the difference is within the 1 σ uncertainties. In this sample we cannot detect clustering on scales $\gtrsim 70h^{-1}$ Mpc. Although the maps of the cluster distribution in redshift space show a large void of diameter $\sim$20,000 km s^{-1}, frequent occurrence of such large empty regions is consistent with the smaller scale behavior of the correlation function of the survey.

Large-scale peculiar motions are $\lesssim$1000 km s^{-1}. This limit is inconsistent with the claim of detection by Bahcall, Soneira, and Burgett of $\sim$2000 km s^{-1} peculiar motions. We suggest that the earlier result is affected by the Corona Borealis supercluster, which contributes more than a third of the excess pairs in the shallower survey.

Subject headings: galaxies: clustering — galaxies: redshifts

I. INTRODUCTION

Galaxy and cluster redshift surveys are two methods of tracing the large-scale distribution of matter in the universe. Comparison of statistics derived from these surveys indicates that clusters of galaxies and individual galaxies are *not* equivalent tracers.

The language of correlation functions provides a quantitative description of the cluster and galaxy distributions. Bahcall and Soneira (1983, hereafter BS) calculated the two-point correlation function for the Hoessel, Gunn, and Thuan (1980) sample of 104 nearby Abell clusters. Postman, Geller, and Huchra (1986, hereafter PGH) calculated the cluster correlation function for a variety of other samples drawn from both the Abell and Zwicky catalogs, and Shectman (1985) analyzed a sample of clusters drawn from the Shane-Wirtanen (1967) counts. For all of these samples the correlation function is consistent with a power law

$$\xi(r) \simeq (r_0/r)^{1.8} . \quad (1)$$

Both the power law and the amplitude r_0 are uncertain. The exponent generally appears to be consistent with the value 1.8 observed for the galaxy correlation function (Peebles 1980; Davis and Peebles 1983; de Lapparent, Geller, and Huchra 1988; Kirshner, Oemler, and Schechter 1979; Shanks *et al.* 1983). With the slope constrained to 1.8, the uncertainty in the amplitude r_0 for a sample of $\sim$150 clusters is $\sim$50%. For the samples analyzed so far,

$$14h^{-1}\ \text{Mpc} \lesssim r_0 \lesssim 25h^{-1}\ \text{Mpc} , \quad (2)$$

where we take the Hubble constant $H_0 = 100h$ km s^{-1} Mpc^{-1} (Bahcall 1988, 1989). In general, the lower values of r_0 are for samples which contain less rich clusters, but the value is also affected by the details of the analysis (see, for example, Sutherland 1988).

One of the concerns about measures of the cluster correlation function is that they are derived from a small number of small samples. We have measured redshifts for 145 clusters in a sample which covers 561 square degrees of the sky and which has a median redshift of 0.16, more than twice the median redshift of the sample analyzed by BS. The new sample has very little overlap with any previous survey. We describe the sample and the data in §§ II and III. We calculate the correlation function in § IV and discuss the effect of contamination by overlapping clusters on these results in § V.

We use the deep cluster sample to explore two other issues: (1) the significance of voids in the distribution of rich clusters and (2) the amplitude of large-scale peculiar motions (Bahcall, Soneira, and Burgett 1986). We discuss the void probability function for the cluster distribution in § VI, and we set limits on peculiar motions in the sample in § VII. Section VIII is a summary of the conclusions which can be drawn from this sample.

II. THE DEEP ABELL CLUSTER SAMPLE

Our deep Abell cluster survey covers a 561 square degree area in the region

$$58° \leq \delta \leq 78° , \quad (3a)$$

$$10^{\rm h} \leq \alpha \leq 15^{\rm h} , \quad (3b)$$

and includes 145 clusters with richness class $R \geq 0$ and distance class $D \leq 6$. The survey region is at high Galactic latitude (96% of the survey area lies north of $b = 40°$). Of the 145 clusters, 137 have $D \geq 5$, and 103 have $R \geq 1$. Redshifts have been measured for all the clusters. Figure 1 shows the distribution of the 145 clusters on the sky.

The effective volume of the deep survey is comparable to that of the $D \leq 4$, $R \geq 1$ sample studied by BS. Although the area covered by the BS sample is $\sim$25 times larger, the deep survey extends $\sim$3 times farther in redshift. Figure 2 shows the

[1] Research reported here is based on observations made with the Multiple Mirror Telescope, a joint facility of the Smithsonian Institution and the University of Arizona, and, in part, on observations made with the Canada-France-Hawaii Telescope operated by the National Research Council of Canada, the Centre National de la Recherche Scientifique of France, and the University of Hawaii.

[2] Harvard-Smithsonian Center for Astrophysics.

[3] Institute for Astronomy, University of Hawaii.

[4] Department of Astrophysical Sciences, Princeton University.

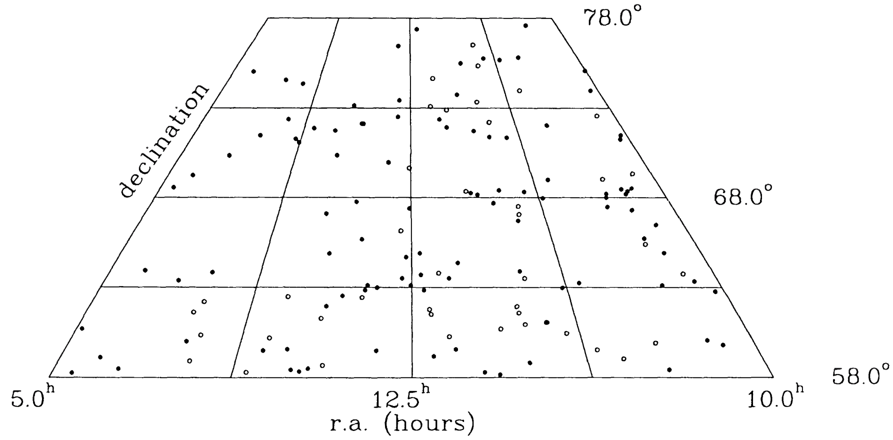

FIG. 1.—Distribution on the sky of the 145 clusters in the deep survey. Open circles represent $R = 0$ clusters; closed circles represent $R \geq 1$ clusters.

radial velocity histograms for the BS sample and for the deep survey. The median redshift for the clusters in the deep survey ($R \geq 1$) is 0.17; the median redshift of the BS sample is 0.07.

Figure 3 shows the mean space density of Abell clusters in the deep survey as a function of redshift. Errors are $(N)^{1/2}$ only. Comoving distances to clusters are computed from redshifts using standard Friedmann cosmology (Mattig 1958):

$$R = \frac{c}{H_0 q_0^2(1+z)} \{q_0 z + (q_0 - 1)[(2q_0 z + 1)^{1/2} - 1]\} . \quad (4)$$

We use $h = 1$ and $q_0 = 0.1$. The survey is seriously incomplete for $z \geq 0.24$, reflecting the incompleteness of the Abell catalog for $z \gtrsim 0.2$ (Lucey 1983). Abell (1958) admits that his survey of $R = 0$ clusters is not statistically complete, and, in fact, there is a significantly higher depletion of $R = 0$ clusters (relative to $R > 0$ clusters) at $z > 0.2$. The redshift histograms for the $R = 0$ and $R > 0$ clusters in our deep survey are consistent, however, for $z \leq 0.2$.

III. SPECTROSCOPIC OBSERVATIONS

a) *MMT Observations*

Spectroscopic measurements were made at the MMT using both the MMT spectrograph (MMTS) with the intensified Reticon photon-counting system (Latham 1982) and the SAO faint-object grism spectrograph (FOGS) equipped with an 800 × 800 TI CCD and the movable multislit assembly (Geary, Huchra, and Latham 1986). With a 300 groove mm^{-1} grating, the MMTS provides a resolution of ~7 Å over the wavelength range 3200–7000 Å. With 300 groove mm^{-1} and 400 groove mm^{-1} grisms, the FOGS provides 15 and 11 Å resolution over the ranges 3800–7500 and 4000–6700 Å, respectively. Velocities were extracted using either the cross-correlation technique (Tonry and Davis 1979) or the positions of the H and K break and/or the blended 3727 Å line of [O II]. The cross-correlation technique was applied to all of the MMTS data, providing velocities (cz, $c = 2.997925 \times 10^5$ km s^{-1}) with external accu-

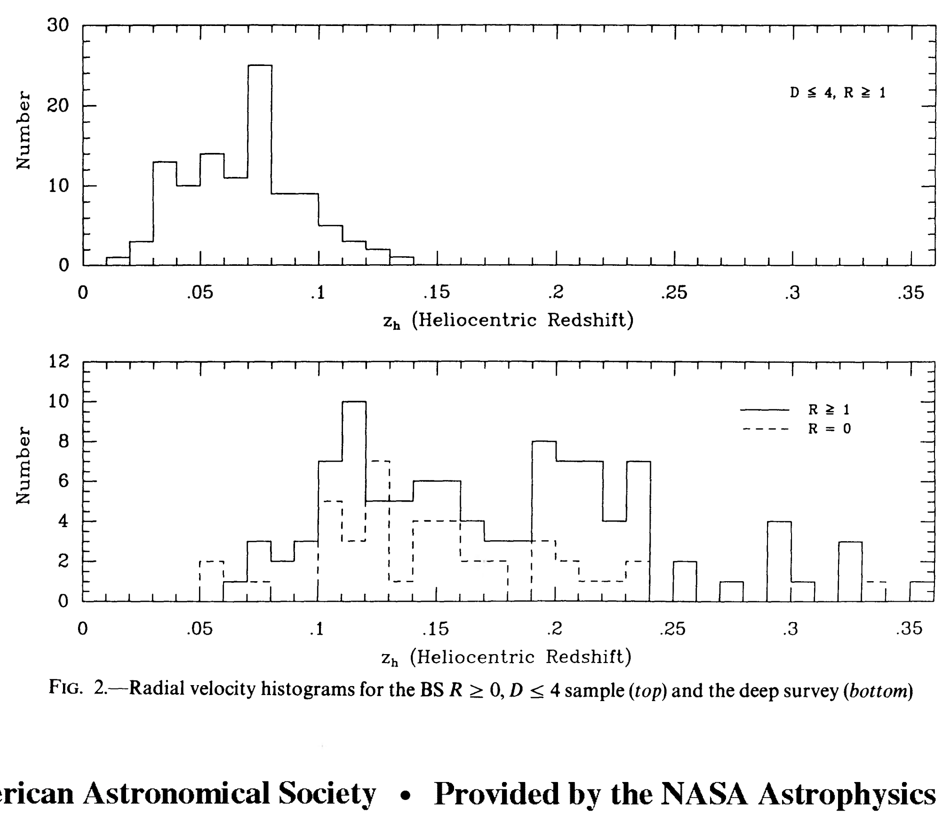

FIG. 2.—Radial velocity histograms for the BS $R \geq 0$, $D \leq 4$ sample (*top*) and the deep survey (*bottom*)

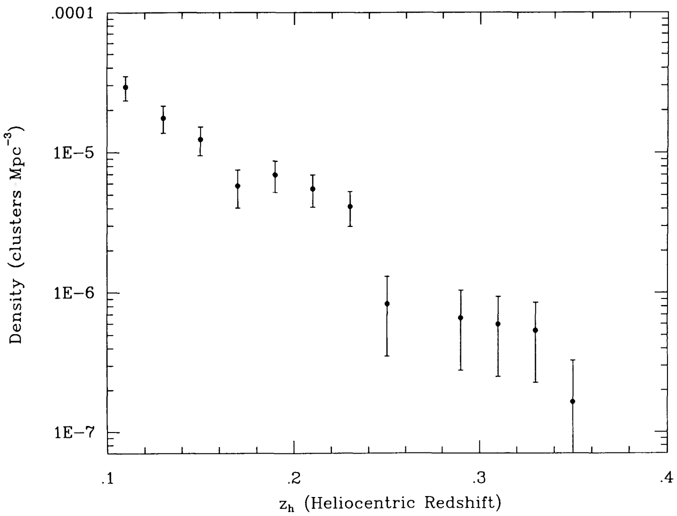

FIG. 3.—Space density of clusters in the deep survey as a function of redshift. Error bars are $\sqrt{N}$ only.

racies of 50–60 km s^{-1}. The cross-correlation technique was applied to some of the FOGS data and yielded accuracies of $\sim$200 km s^{-1}. Velocities measured from the H + K break in lower signal-to-noise FOGS data have accuracies of $\sim$200 km s^{-1}.

b) CFHT and Hawaii 2.2 m *Observations*

Data were acquired with the Hawaii grism spectrograph mounted at the Cassegrain focus of either the Canada-France-Hawaii 3.6 m telescope of the University of Hawaii 2.2 m telescope. We used the *Galileo* IfA CCD, a 500 × 500 TI thinned device. This configuration provided 15 Å resolution over the range 4400–6400 Å. Exposures were generally 15 minutes. We use standard procedures for the reduction of long-slit CCD spectroscopy. The reduction procedure consists of bias subtraction, flat-fielding, extraction of the object and sky spectra, and wavelength linearization. Redshifts were determined from prominent features such as Ca II H and K, the G band, and Mg *b*. The internal accuracy of the redshifts, judged from the dispersion of individual features, is about 300 km s^{-1}.

c) Summary

Table 1 summarizes the cluster data. Column (1) is the Abell (1958) number. Supplementary comments are given in the notes to Table 1. Columns (2) and (3) are Abell's estimates of the 1950 right ascension and declination of the cluster center, columns (4) and (5) give the Abell richness and distance class, columns (6) and (7) give the magnitudes of the first and 10 brightest galaxies, column (8) is the estimated cluster redshift from Leir and van den Bergh (1977), and column (9) is the actual *heliocentric* cluster redshift, either from our measurements or, in a few cases, from the literature. The number of redshift measurements used to compute the mean cluster redshift and the references for the redshift measurements are in columns (10) and (11), respectively. Eleven clusters in our sample also have redshifts determined by Ciardullo, Ford, and Harms (1985). We agree on the redshifts of eight of these (average deviation $z = 0.0000$), but there is serious disagreement for A1859, A1877, and A1975 (see notes to Table 1). The redshifts for A1559, A1674, and A1918 have been measured by us and by Schneider, Gunn, and Hoessel (1983) with good agreement. In both Tables 1 and 2, redshifts measured by J. H. at Mount Hopkins are designated "JH," and those measured by P. H. at Mauna Kea are designated "PH." Redshifts from several other literature sources are also given.

Table 2 is a list of the velocities for the individual galaxies observed in this program. The table includes the galaxy IAU name (col. [1]), the coordinates (cols. [2] and [3]) accurate to $\pm 15''$, the heliocentric redshift (col. [4]), the heliocentric velocity (col. [5]), the error in the velocity, *cz* (col. [6]), and other designations and comments (col. [7]). The Abell cluster number precedes each set of data at the far left. When measurements of the same galaxy exist, with one exception, our redshifts are in good agreement with values in the literature and with each other. In the case of A1865, we have used the redshifts determined by P. H., since the two discordant redshifts of J. H. are of very low quality.

Perhaps surprisingly, the problems of significant foreground and background contamination exist for all richness and distance classes in our sample. Because we do not sample all the clusters equally well, we cannot treat the interloper problem in a uniform way. In the table notes we consider the issue on a case-by-case basis. In many cases it is not easy to select a single redshift for the cluster. This problem is especially acute for distant, poor clusters contaminated by individual galaxies and groups of galaxies in the foreground and/or background. We comment on the worst cases in the notes to Table 1 (also see the discussion in § V). Of the 90 clusters in the sample where we have measured more than one redshift, 40% (36 clusters) show multiple redshift systems or significant (≥ 5000 km s^{-1}) extent in redshift space. In these cases, the redshifts in Table 1 are only a best guess for Abell's "cluster." Accidentally choosing a foreground redshift tends to bias the amplitude of the cluster correlation function toward larger values (see PGH).

IV. THE SPATIAL CORRELATION FUNCTION

We use the two point spatial correlation function to describe clustering in the deep survey. A Monte Carlo estimator is the optimal choice for minimizing edge effects. The estimator for the spatial correlation function is

$$\xi(r) = \frac{N_p(r)}{N_r(r)} - 1 , \qquad (5)$$

where $N_p(r)$ is the number of cluster pairs in the deep survey with separations between $r - \Delta r/2$ and $r + \Delta r/2$, $N_r(r)$ is the number of pairs in a random distribution of clusters over an identical area. Spatial separations are based on comoving distances derived from redshifts (eq. [4]). We average the number of random pairs at each separation over 50 simulations. The slope and amplitude of the correlation function do not change significantly if we increase the number of simulations 10-fold. We use logarithmic bins in spatial separation with $\Delta \log r = 0.1$. Logarithmic bins improve the signal-to-noise ratio at large separations where the amplitude of the correlation function is small. Our results, however, do not change significantly with linear binning. We obtain the redshift distribution for the random catalogs by choosing redshifts at random from the *real* survey and "smoothing" with a small random Gaussian ($\sigma = 0.01$ in z) to prevent reproduction of small-scale clumpiness in the actual redshift distribution. We use the Galactic latitude selection function $P(b) = 10^{0.3(1 - \csc|b|)}$, a good fit to the observed selection function of the Abell catalog. Reasonable variations have negligible effect. There is no significant declination selection bias in the Abell catalog in this part of the sky.

Figure 4 shows the spatial correlation functions for all 145

TABLE 1

DEEP ABELL CLUSTER CATALOG

Abell	R.A. 1950	Dec	R	D	m_1	m_{10}	z_{est}	z_{obs}	N	Ref
909	10 00.6	+75 05	2	6	17.60	17.70	0.2250	0.2947	2	JH
914	10 04.3	+71 29	2	6	18.20	17.70	0.2520	0.1941	3	JH
917	10 04.3	+62 46	1	6	16.70	17.40	0.1740	0.1320	3	PH
918	10 06.1	+73 59	1	5	17.60	17.10	0.1680	0.1661	1	JH
922	10 06.3	+71 16	2	6	16.60	17.90	0.2110	0.1890	3	JH
945	10 11.8	+69 21	0	5		17.20		0.1982	1	JH
947	10 11.6	+63 20	1	5	16.60	16.80	0.1380	0.1766	2	JH
948	10 12.9	+72 34	0	5		17.10		0.1207	2	JH
959	10 14.1	+59 49	1	6	17.90	17.80	0.2740	0.3530	2	PH
960	10 15.1	+66 29	2	5	16.10	17.20	0.1610	0.1290	1	PH
962	10 15.3	+63 44	0	5		17.10		0.1692	2	JH
968	10 17.4	+68 32	2	6	16.80	17.50	0.2000	0.1949	1	JH
975	10 19.1	+64 53	2	5	15.90	16.80	0.1260	0.1182	2	JH
981	10 20.7	+68 22	2	6	16.90	17.90	0.2040	0.2013	1	JH
983	10 20.1	+60 04	2	6	16.20	17.70	0.1630	0.2055	2	PH
998	10 22.6	+68 13	2	6	16.90	17.50	0.1900	0.2026	5	JH
1005	10 23.9	+68 29	2	6	17.40	17.50	0.2030	0.1998	2	JH
1006	10 24.0	+67 18	1	6	16.90	17.70	0.2150	0.2039	3	PH,JH
1014	10 25.5	+65 42	2	5	16.40	17.10	0.1540	0.1161	1	JH
1017	10 26.6	+65 23	0	6		17.90		0.2030	1	PH
1025	10 28.2	+63 07	2	5	16.90	16.90	0.1560	0.1508	2	JH
1029	10 31.0	+77 36	2	5	15.90	17.10	0.1350	0.1258	2	JH
1037	10 32.1	+69 03	0	6		17.70		0.3075	2	PH
1046	10 34.0	+68 14	2	6	17.10	17.50	0.2060	0.1895	2	PH
1049	10 35.1	+68 01	2	6	17.90	17.70	0.2570	0.2575	2	PH,JH
1061	10 37.3	+67 29	2	6	17.00	17.70	0.2320	0.1886	5	JH
1076	10 41.9	+58 26	1	5	16.10	17.20	0.1510	0.1164	2	JH
1083	10 43.1	+59 55	0	6		17.60		0.2240	2	PH
1123	10 52.9	+75 48	2	5	15.50	16.90	0.1200	0.1221	2	SG
1124	10 52.6	+72 02	2	6	17.50	17.30	0.2120	0.2231	2	JH
1144	10 59.4	+59 02	0	5		17.20		0.1507	1	JH,PH
1150	11 02.8	+73 58	0	5		16.50		0.1202	2	JH
1166	11 05.9	+69 01	1	5	16.90	17.10	0.1590	0.1639	1	JH
1180	11 08.1	+63 14	1	6	16.10	17.80	0.1630	0.0900	2	PH
1186	11 10.4	+75 40	2	5	15.90	16.50	0.1350	0.0785	2	SRS
1192	11 09.6	+59 32	0	6		17.60		0.1980	1	PH
1207	11 12.6	+67 58	1	5	16.30	17.10	0.1550	0.1351	1	JH
1221	11 16.9	+62 58	1	6	15.10	17.60	0.1470	0.2120	1	PH
1239	11 21.1	+60 26	0	6		17.50		0.1670	2	PH
1249	11 22.4	+68 19	1	5	15.90	17.20	0.1550	0.1558	1	JH
1254	11 23.8	+71 22	1	3	13.60	15.30	0.0490	0.1520	1	JH
1255	11 24.4	+75 46	1	5	16.10	16.70	0.1300	0.1650	2	JH,PH
1279	11 28.3	+67 31	0	5		16.50		0.0548	2	JH
1283	11 28.4	+61 03	1	5	16.70	17.20	0.1850	0.1404	3	JH,PH,CFH
1287	11 28.9	+67 04	0	5		17.00		0.1432	2	JH
1289	11 28.8	+61 03	0	5		17.00		0.1114	3	JH
1297	11 30.6	+76 31	0	4		16.10		0.1248	2	JH
1301	11 30.8	+75 21	0	5		16.50		0.1218	2	JH
1302	11 30.5	+66 42	2	5	15.20	16.70	0.1150	0.1160	3	JH,RK
1315	11 33.2	+72 13	0	5		16.50		0.1409	2	JH
1322	11 34.2	+63 30	0	5		17.20		0.1110	4	JH,CFH
1329	11 35.7	+71 24	1	5	14.70	16.50	0.1050	0.1453	1	JH
1331	11 36.0	+63 52	2	6	16.50	17.60	0.1940	0.2093	7	JH,PH
1335	11 37.3	+68 25	1	5	16.10	17.20	0.1710	0.1500	1	JH
1339	11 38.7	+73 21	0	6		17.40		0.1556	1	JH
1343	11 38.6	+60 56	0	5		17.20		0.1313	2	CFH,JH
1351	11 39.8	+58 49	2	6	17.20	17.80	0.3140	0.3220	3	PH
1357	11 40.3	+61 34	0	5		16.90		0.1707	3	PH
1359	11 40.8	+61 56	0	5		17.20		0.1786	2	JH,CFH
1366	11 42.2	+67 42	1	5	15.80	16.80	0.1360	0.1159	1	JH
1381	11 45.7	+75 30	2	5	15.80	17.00	0.1340	0.1165	1	JH
1382	11 45.6	+71 43	1	4	14.90	15.90	0.0820	0.1048	2	HGT,HSM
1402	11 49.9	+60 42	0	5		17.20		0.1058	2	JH
1406	11 50.6	+68 10	1	5	15.80	17.20	0.1570	0.1173	1	JH
1412	11 53.1	+73 45	2	4	15.30	15.90	0.0950	0.0834	1	HGT,JH
1415	11 53.2	+58 09	1	5	16.30	17.00	0.1550	0.1587	3	JH
1421	11 54.4	+68 15	1	5	16.90	17.20	0.1820	0.1182	2	JH
1432	11 57.1	+68 23	0	6		17.70		0.1130	1	PH
1446	11 59.3	+58 18	2	5	15.30	17.00	0.1180	0.1031	2	JH
1467	12 02.9	+72 53	0	6		17.40		0.1034	2	JH
1470	12 04.4	+71 55	2	6	16.20	17.40	0.1620	0.1912	3	JH
1477	12 06.4	+64 21	1	6	16.20	18.00	0.2430	0.1104	1	JH,PH
1484	12 08.7	+72 22	1	6	15.80	17.40	0.1480	0.1220	3	JH
1496	12 10.9	+59 33	1	4	15.40	16.00	0.0900	0.0957	1	HGT
1500	12 11.5	+74 40	0	3		15.60		0.0714	2	JH
1501	12 11.7	+63 30	1	5	16.70	17.20	0.1850	0.1305	2	PH

TABLE 1—*Continued*

Abell	R.A. 1950	Dec	R	D	m_1	m_{10}	z_{est}	z_{obs}	N	Ref
1507	12 13.4	+60 15	0	4	15.20	15.80	0.0870	0.0602	5	JH
1513	12 14.7	+73 06	0	5		17.10		0.1524	1	JH
1518	12 16.6	+63 47	0	5		17.00		0.1080	1	JH
1528	12 20.5	+59 11	1	6	17.00	17.80	0.2010	0.1540	2	PH
1529	12 20.9	+61 30	0	6		18.00		0.2320	1	PH
1534	12 21.7	+61 47	0	5		17.00		0.0698	3	JH
1536	12 22.8	+77 24	1	5	16.10	16.90	0.1600	0.1238	2	JH
1539	12 24.0	+62 50	2	5	16.60	17.20	0.1670	0.1707	1	JH
1544	12 25.4	+63 42	1	5	16.00	17.20	0.1590	0.1454	1	JH
1546	12 25.7	+64 53	2	6	17.90	18.00	0.2490	0.2330	1	PH
1557	12 30.3	+63 07	2	6	17.90	18.00	0.2930	0.2100	2	PH
1559	12 30.9	+67 24	1	5	14.80	17.20	0.1170	0.1066	2	JH,SG
1561	12 31.0	+69 39	0	6		17.40		0.1105	2	JH
1566	12 32.8	+64 40	2	6	16.00	16.90	0.1460	0.1000	2	PH
1576	12 34.6	+63 29	3	6	17.20	18.00	0.2790	0.3020	1	PH
1579	12 35.7	+66 08	0	6		17.60		0.2000	1	PH
1590	12 38.2	+73 26	1	5	14.90	16.80	0.1000	0.2249	1	JH
1597	12 39.1	+72 31	1	6	15.80	17.50	0.2050	0.1096	1	JH
1607	12 41.0	+76 26	2	5	15.90	16.70	0.1310	0.1355	1	JH,RK
1614	12 44.3	+69 58	1	6	17.60	17.50	0.2530	0.2320	1	PH
1617	12 45.4	+59 29	3	6	17.20	17.60	0.2260	0.1520	1	PH
1621	12 46.6	+62 58	1	5	15.80	16.50	0.1150	0.1029	4	JH,PH,RK
1636	12 51.4	+63 06	2	6	15.90	17.80	0.1810	0.2350	2	PH
1640	12 52.4	+62 50	1	6	16.10	17.80	0.1780	0.1250	1	PH
1646	12 53.7	+62 26	0	5		16.90		0.1063	1	JH
1655	12 56.3	+65 39	2	6	17.70	18.00	0.2580	0.2340	1	PH
1674	13 01.7	+67 46	3	5	15.90	17.20	0.1550	0.1060	2	JH,SG
1678	13 03.0	+62 31	1	6	16.60	17.40	0.1900	0.1700	2	PH
1681	13 03.4	+72 08	1	5	15.70	17.10	0.1460	0.0906	2	JH
1683	13 04.6	+72 08	1	5	17.40	17.10	0.1950	0.1335	1	JH
1687	13 07.8	+58 41	0	6		17.50		0.1950	2	PH
1695	13 09.9	+61 57	1	6	16.70	17.80	0.1950	0.1970	1	PH
1701	13 11.6	+61 17	0	5		17.00		0.1234	1	JH
1704	13 12.6	+64 52	3	6	16.50	17.80	0.2350	0.2200	1	PH
1705	13 12.3	+73 09	1	6	17.40	17.70	0.2360	0.2960	1	PH
1707	13 13.7	+58 30	1	6	16.90	17.60	0.2250	0.1960	1	PH
1713	13 17.2	+58 21	1	5	15.60	17.20	0.1430	0.1406	1	JH
1718	13 17.8	+67 07	2	6	15.90	17.80	0.1580	0.3340	1	PH
1722	13 18.2	+70 22	2	6	18.20	17.70	0.2640	0.3275	1	PH
1731	13 20.8	+58 26	2	5	15.90	17.20	0.1470	0.1945	1	JH
1741	13 22.7	+71 44	1	5	15.70	17.10	0.1310	0.0739	2	JH,PH
1744	13 24.0	+59 34	1	5	15.70	17.20	0.1750	0.1515	1	JH
1756	13 28.7	+62 29	0	6		17.60		0.2410	1	PH
1764	13 32.9	+60 11	0	5		17.20		0.1167	2	JH
1767	13 34.2	+59 29	1	4	14.10	15.70	0.0690	0.0701	16	HH+
1776	13 39.2	+58 17	0	5		17.20		0.1330	1	JH
1777	13 38.2	+71 52	1	6	17.10	17.60	0.2400	0.2150	2	JH
1803	13 45.5	+71 05	1	6	16.70	17.50	0.1980	0.1997	1	JH
1811	13 48.7	+71 17	1	6	16.90	17.50	0.1940	0.1162	4	JH
1848	13 57.5	+74 22	1	6	17.30	17.70	0.2400	0.1994	1	JH
1851	13 58.5	+72 22	2	5	16.60	17.20	0.1920	0.2143	3	JH
1859	14 03.6	+60 21	0	6		17.80		0.2353	5	JH
1865	14 04.3	+58 55	0	6		17.80		0.2173	3	JH
1872	14 07.6	+62 12	0	5		17.20		0.1431	3	JH,PH.CFH
1877	14 08.9	+60 01	1	6	16.40	17.80	0.2010	0.2493	2	JH
1879	14 09.1	+63 50	1	6	16.70	17.80	0.2180	0.2055	2	PH
1884	14 10.4	+61 37	0	6		17.80		0.1217	3	JH
1893	14 12.6	+74 34	1	6	17.30	17.50	0.2090	0.2065	2	PH
1895	14 13.7	+71 28	2	6	17.60	17.70	0.2430	0.2250	1	PH
1918	14 23.9	+63 23	3	6	15.40	17.50	0.1690	0.1394	4?	SG,CFH,DJ
1933	14 28.4	+70 22	2	6	16.20	17.30	0.1820	0.2118	3	JH
1937	14 33.0	+58 30	2	5	16.80	17.20	0.1930	0.1379	2	JH,CFH
1966	14 42.8	+59 07	2	6	16.70	18.00	0.2560	0.1500	2	PH
1969	14 42.8	+63 55	1	6	17.10	17.70	0.2310	0.2981	1	JH
1974	14 43.3	+75 03	1	6	17.10	17.50	0.2010	0.1769	5	JH
1975	14 44.9	+69 15	1	5	16.50	17.10	0.1540	0.2228	1	JH
1995	14 51.5	+58 16	1	7		18.40		0.3180	2	PH
2002	14 52.4	+68 35	1	6	17.60	17.70	0.2390	0.2110	1	PH
2013	14 57.6	+60 42	2	6	17.10	18.00	0.2690	0.2395	2	PH

survey clusters, for the 103 $R \geq 1$ clusters, and for the 132 clusters with $z \leq 0.24$. The least-squares power-law fits with slope constrained to -1.8 are

$$\xi(r) = \left(\frac{r}{20.3h^{-1}\ \mathrm{Mpc}}\right)^{-1.8}, \quad R \geq 0\ , \tag{6a}$$

$$\xi(r) = \left(\frac{r}{20.9h^{-1}\ \mathrm{Mpc}}\right)^{-1.8}, \quad R \geq 1\ , \tag{6b}$$

$$\xi(r) = \left(\frac{r}{20.7h^{-1}\ \mathrm{Mpc}}\right)^{-1.8}, \quad z \leq 0.24\ . \tag{6c}$$

We fit over the range $10h^{-1}$ Mpc $\leq r \leq 70h^{-1}$ Mpc. The 1 σ uncertainties in these correlation lengths are $(+4.79, -5.05)$ h^{-1} Mpc, $(+6.69, -6.91)h^{-1}$ Mpc, and $(+6.32, -6.38)h^{-1}$ Mpc for the $R \geq 0$, $R \geq 1$, and $z \leq 0.24$ samples, respectively. We use the bootstrap resampling technique (Ling, Frenk, and Barrow 1986) to estimate the uncertainties. Because of the small sample of clusters, the error in the determination of $\xi(r)$ is large for $r \gtrsim 70h^{-1}$ Mpc. Therefore we cannot reliably detect clustering on larger scales. We also create two independent subsamples by splitting the entire survey at the median redshift of $z = 0.1534$. The least-squares power-law fits with slope constrained to -1.8 are

$$\xi(r) = \left(\frac{r}{19.8h^{-1}\ \mathrm{Mpc}}\right)^{-1.8}, \quad z \leq 0.1524\ , \tag{6d}$$

$$\xi(r) = \left(\frac{r}{23.5h^{-1}\ \mathrm{Mpc}}\right)^{-1.8}, \quad z > 0.1524\ . \tag{6e}$$

The scatter in the correlation function for these last two sub-

NOTES TO TABLE 1

Redshift references.—JH = this paper, Mount Hopkins; PH = this paper, Mauna Kea; F = Fetisova 1982; CFH = Ciardullo, Ford, and Harms 1985; HGT = Hoessel, Gunn, and Thuan 1980; HSM = Hoessel, Gunn, and Thuan 1980; HSM = Hintzen, Scott, and McKee 1980; SGH = Schneider, Gunn, and Hoessel 1988; Schneider 1983; SRS = Sarazin, Rood, and Struble 1982; DJ = Jenner 1974; RK = Rhee and Katgert 1988; HH + = Hintzen *et al.* 1982; OWT = Owen, White, and Thronson 1988.

Notes on Individual Clusters

A909.—Complex field with several redshift systems; brightest galaxy is probably foreground.

A918.—Cluster not well defined.

A998.—Brightest pair is foreground double.

A1005.—Cluster velocity uncertain.

A1037.—Cluster confused; we have adopted the high redshift, but the correct redshift may be $z = 0.154$.

A1046/1049.—Confused cluster pair; we have adopted PH's low redshift for A1046 and PH's and JH's high redshift for A1049.

A1124.—Complex field; also galaxies at $z = 0.19$ and $z = 0.43$ and foreground contamination.

A1180.—We have adopted $z = 0.09$; there are also galaxies at $z = 0.14$ and $z = 0.24$. This cluster needs more work.

A1186.—SRS quote an unpublished redshift for this cluster based on one galaxy; here we assume they measured the brightest galaxy in the field, and in Table 2 we include coordinates for a second galaxy.

A1254.—Complex field with foreground groups plus a real, rich cluster at moderately high redshift. Previous cluster redshift from HGT is for one of the foreground groups; Abell's coordinates roughly centered on the cluster at $z = 0.15$. This field needs more work.

A1283/1289.—Abell identified two clusters almost on top of each other. Surprisingly, there are two distinct concentrations in redshift space, one at $z = 0.14$ that we tentatively identify with A1283 and one at $z = 0.11$ that we identify with A1289.

A1297.—Brightest galaxy is foreground.

A1329.—Brightest galaxy is foreground.

A1343.—Foreground group superposed.

A1357.—Seyfert 2 galaxy is several thousand km s^{-1} off cluster mean.

A1351.—Given cluster redshift is the average of three fairly well separated redshifts (8000 km s^{-1}); cluster needs more work.

A1402.—Confused field.

A1412.—Confused field; we adopt the redshift for the brightest galaxy from HGT; however, the second brightest is at a redshift only 7000 km s^{-1} higher.

A1467.—Brightest galaxy in field is edge on spiral and foreground.

A1477.—Two of the brighter galaxies in the field have $z \sim 0.1$; the densest concentration of galaxies may be at higher redshift.

A1500.—Arp's favorite Seyfert galaxy, Markarian 205, is at the same redshift as brightest galaxy at the cluster center.

A1507.—Confused field; the large concentration of galaxies that is centered to the southwest of the Abell center is at $z = 0.06$; a smaller concentration to the northeast is at $z = 0.04$.

A1518.—We adopt the redshift of the brightest galaxy in field, which is also close to the estimated z; there also are galaxies at $z = 0.135$ and $z = 0.039$.

A1557.—PH measured two galaxies at the same redshift.

A1561.—Very (!) confused field; we have redshifts for five galaxies, only two of which agree. We have adopted that as the cluster redshift.

A1597.—We adopt for the cluster redshift that of the brightest galaxy in the field, which is also at the apparent cluster center; there is also a galaxy at $z = 0.076$

A1681/1683.—A1683 and A1681 are on top of each other, and one or the other of these clusters may not really exist (cf. § V). Two of the galaxies in the field are at $z = 0.09$ and are near the assumed center of A1681; two other galaxies in the field are at much higher (and different) redshifts. We adopt the lower of those two for A1683, but this needs to be checked. There are no galaxies at Abell's center for A1683.

A1713.—Redshift adopted is for the second brightest galaxy in the field, which is the galaxy closest to the Abell center and near the estimated redshift. The brightest galaxy in the field is off the cluster center but is only at a redshift 0.04 below the second brightest galaxy. Thus, the cluster redshift is possibly $z = 0.10$.

A1756.—We have adopted the lower of the two redshifts in the field; there is also a galaxy at $z = 0.24$.

A1851.—Confused field with at least two foreground groups.

A1859.—CFH redshift is for a foreground galaxy far from Abell's cluster center.

A1865.—PH's and JH's redshifts are discrepant for the same galaxies; we have adopted PH's, since JH's are of low quality. This cluster redshift needs to be confirmed.

A1877.—Confused field; CFH redshift probably for foreground galaxy; there are several other systems in the field. We have adopted the redshift closest to the estimated redshift. This cluster needs more work.

A1884.—The galaxy at $z = 0.17$ is probably background.

A1893.—Sparse field with at least two galaxies near estimated cluster redshift.

A1918.—Coordinates for 1424+6331 from Palumbo, Tanzella-Nitti, and Vettolani 1983 may be wrong; the dumbbell galaxy measured by Jenner 1974 is probably the one at the cluster center. There is some confusion over the published coordinates for galaxies in this field, but the cluster redshift is probably correct.

A1969.—Complex field. We adopt as the cluster redshift that of the D galaxy nearest the coordinate center.

A1975.—CFH redshift is for a foreground galaxy far from the coordinate center.

TABLE 2

INDIVIDUAL GALAXY REDSHIFTS[a]

Name	α (1950)	δ	Z	V_h	σ		Comments
A 909							
1001+7503A	10:01:20.6	75:03:03	0.2927	87740	300	JH	
1001+7503B	10:01:21.4	75:02:55	0.2967	88950	300	JH	
1001+7501	10:01:46.0	75:01:40	0.1879	56330	300	JH	
1001+7506	10:01:53.7	75:06:24	0.2182	65400	150	JH	Poor velocity
A 914							
1005+7126A	10:05:21.5	71:26:00	0.1949	58440	220	JH	
1005+7126B	10:05:25.4	71:26:05	0.1965	58924	250	JH	
1005+7125	10:05:31.4	71:25:50	0.1909	57240	300	JH	
A 917							
1004+6244A	10:04:39.1	62:44:39	0.1330	39860	300	PH	
1004+6244B	10:04:42.4	62:44:40	0.1320	39560	300	PH	
A 918							
1006+7404	10:06:35.0	74:04:56	0.1661	49800	63	JH	
A 922							
1006+7115	10:06:09.5	71:15:25	0.2710	81230	220	JH	
1006+7116A	10:06:17.3	71:16:33	0.1891	56697	165	JH	
1006+7116B	10:06:23.3	71:16:20	0.1893	56760	260	JH	
1006+7117	10:06:27.2	71:17:07	0.1885	56523	233	JH	
A 945							
1011+6923	10:11:57.0	69:23:39	0.1982	59414	54	JH	
1011+6924	10:11:59.0	69:24:14	0.0344	10314	38	JH	Foreground
A 947							
1011+6320	10:11:46.0	63:20:20	0.1757	52663	49	JH	
1011+6319	10:11:33.0	63:19:50	0.1775	53221	63	JH	
A 948							
1013+7235	10:13:33.0	72:35:27	0.1211	36291	39	JH	
1013+7236	10:13:57.5	72:36:11	0.1204	36094	40	JH	
A 959							
1014+5947A	10:14:09.5	59:47:02	0.3509	105195	300	PH	
1014+5947B	10:14:11.0	59:47:03	0.3549	106390	300	PH	
A 960							
1015+6629	10:15:06.1	66:29:44	0.1290	38660	300	PH	
A 962							
1014+6342	10:14:56.0	63:42:12	0.1749	52428	50	JH	
1015+6346	10:15:23.0	63:46:55	0.1636	49034	44	JH	
A 968							
1017+6836A	10:17:44.1	68:36:34	0.1949	58440	187	JH	
A 975							
1019+6451	10:19:24.0	64:51:00	0.1179	35346	51	JH	
1020+6455	10:20:06.0	64:55:00	0.0403	12070	42	JH	Foreground
1020+6452	10:20:12.0	64:52:00	0.1184	35498	53	JH	
A 981							
1020+6820	10:20:36.0	68:20:06	0.2013	60357	74	JH	
A 983							
1019+6004	10:19:51.5	60:04:26	0.2069	62038	300	PH	
1019+6005	10:19:58.6	60:05:02	0.2039	61140	300	PH	
A 998							
1022+6810A	10:22:36.0	68:10:58	0.0385	11546	41	JH	Foreground
1022+6810B	10:22:37.0	68:10:50	0.0374	11213	100	JH	Foreground
1022+6810C	10:22:42.0	68:10:20	0.1935	57998	222	JH	
1022+6814	10:22:46.0	68:14:41	0.2094	62770	64	JH	
1022+6811	10:22:47.0	68:11:12	0.1971	59099	225	JH	
1022+6810D	10:22:51.0	68:10:02	0.2032	60906	316	JH	
1022+6809	10:22:53.0	68:09:50	0.2099	62940	300	JH	

TABLE 2—*Continued*

Name	α (1950)	δ	Z	V_h	σ		Comments
A1005							
1023+6827A	10:23:32.0	68:27:16	0.2002	60024	250	JH	Poor velocity
1023+6829	10:23:48.0	68:29:12	0.2369	71030	175	JH	
1023+6827B	10:23:48.0	68:27:20	0.1993	59751	290	JH	Poor velocity
A1006							
1023+6717A	10:23:58.7	67:17:13	0.1924	57695	171	JH	V=57840 PH
1024+6718	10:24:12.0	67:18:02	0.2072	62104	180	JH	Poor velocity
1024+6717B	10:24:21.5	67:17:57	0.2122	63623	262	JH	Poor velocity
A1014							
1025+6539	10:25:38.0	65:39:25	0.1161	34810	74	JH	
A1017							
1026+6520	10:26:44.1	65:20:14	0.2029	60840	300	PH	
A1025							
1028+6308	10:28:18.0	63:08:15	0.1502	45042	42	JH	
1028+6307	10:28:19.0	63:07:41	0.1513	45358	54	JH	
A1029							
1029+7738	10:29:20.0	77:38:07	0.1260	37764	42	JH	
1031+7735	10:31:42.0	77:35:06	0.1256	37646	35	JH	
A1037							
1032+6900A	10:32:02.6	69:00:20	0.3099	92910	300	PH	
1032+6900B	10:32:04.0	69:00:40	0.3049	91410	300	PH	
1032+6901	10:32:09.9	69:01:54	0.1541	46186	44	JH	Foreground??
A1046							
1033+6814A	10:33:28.1	68:14:06	0.1889	56640	300	PH	
1033+6814B	10:33:42.5	68:14:03	0.1899	56940	300	PH	
1034+6812A	10:34:03.0	68:12:08	0.2550	76459	268	JH	Possible member of 1049
1034+6812B	10:34:21.0	68:12:43	0.2377	71254	223	JH	Possible member of 1049
A1049							
1035+6801A	10:35:14.1	68:01:07	0.2599	77920	300	PH	
1035+6801B	10:35:27.5	68:01:01	0.2419	72530	300	PH	
A1061							
1037+6729A	10:37:04.4	67:29:52	0.1926	57731	159	JH	
1037+6729B	10:37:13.3	67:29:24	0.1909	57239	173	JH	
1037+6729C	10:37:19.7	67:29:49	0.1900	56974	280	JH	
1037+6730	10:37:15.0	67:30:33	0.1777	53264	84	JH	
1037+6729D	10:37:31.7	67:29:42	0.1918	57505	206	JH	
A1076							
1042+5824	10:42:04.0	58:24:19	0.1174	35198	46	JH	
1042+5823	10:42:01.0	58:23:41	0.1153	34576	32	JH	
A1083							
1043+5954	10:43:03.4	59:54:19	0.2239	67130	300	PH	
1043+5953	10:43:14.8	59:53:25	0.2239	67130	300	PH	
A1123							
1052+7546	10:52:59.0	75:46:27	0.1230	36868	300	SGH	
1053+7546	10:53:01.0	75:46:27	0.1212	36328	300	SGH	
A1124							
1053+7201	10:53:23.8	72:01:49	0.2236	67033	287	JH	
1053+7200A	10:53:23.9	72:00:58	0.2226	66745	237	JH	
1053+7200B	10:53:25.0	72:00:53	0.0695	20847	228	JH	Poor velocity
1053+7202	10:53:39.0	72:02:02	0.1900	56972	191	JH	
1053+7200C	10:53:39.3	72:00:59	0.4318	129443	271	JH	Poor velocity
1053+7200D	10:53:54.5	72:00:59	0.3337	100026	224	JH	Poor velocity
1053+7200E	10:53:59.0	72:00:34	0.1050	31465	297	JH	Poor velocity
A1144							
1059+1410	10:59:31.8	58:59:34	0.0481	14426	61	JH	Foreground
1059+5902	10:59:31.8	59:02:32	0.1687	50567	73	JH	V=50050 PH
1059+5903	10:59:32.9	59:03:53	0.1507	45170	49	JH	V=43460 PH

TABLE 2—*Continued*

Name	α (1950)	δ	Z	V_h	σ		Comments
A1150							
1103+7353	11:03:15.6	73:53:26	0.1205	36130	50	JH	
1103+7355	11:03:36.2	73:55:17	0.1341	40188	46	JH	
1103+7357	11:03:45.7	73:57:58	0.1199	35957	60	JH	
A1166							
1106+6859	11:06:23.0	68:59:12	0.1639	49129	36	JH	
A1180							
1109+6317A	11:09:04.1	63:17:47	0.1410	42260	300	PH	
1109+6317B	11:09:05.8	63:17:22	0.2419	72530	300	PH	
1109+6317C	11:09:07.7	63:17:04	0.0900	26970	300	PH	
1109+6316	11:09:08.0	63:16:39	0.0900	26970	300	PH	
A1186							
1110+7541	11:10:34.1	75:41:39	0.0785	23540	300	SRS	???
1110+7542	11:10:26.6	75:42:57					
A1192							
1109+5931A	11:09:54.9	59:31:47	0.0290	8691	300	PH	Foreground
1109+5931B	11:09:49.8	59:31:28	0.1979	59340	300	PH	
A1207							
1112+6755	11:12:15.0	67:55:48	0.1351	40511	38	JH	
A1221							
1116+6300	11:16:35.1	63:00:21	0.2119	63540	300	PH	
A1239							
1120+6020A	11:20:54.9	60:20:42	0.1669	50050	300	PH	
1120+6020B	11:20:58.6	60:20:21	0.1669	50050	300	PH	
A1249							
1122+6819	11:22:31.0	68:19:59	0.1558	46715	51	JH	
A1254							
1122+7111A	11:22:02.2	71:11:23	0.0625	18750	37	JH	= HGT-1
1122+7111B	11:22:27.5	71:11:46	0.0437	13115	33	JH	
1124+7123	11:24:29.9	71:23:51	0.1520	45564	46	JH	
A1255							
1124+7546A	11:24:56.0	75:46:15	0.1629	48850	300	JH	Poor velocity
1123+7546B	11:24:58.4	75:46:08	0.1669	50050	300	PH	
A1279							
1128+6731A	11:28:18.0	67:31:30	0.0549	16460	104	JH	
1128+6731B	11:28:47.0	67:31:30	0.0547	16397	36	JH	
A1283/8							
1128+6103	11:28:43.0	61:03:39	0.1434	42990	100	CFH	Coords off
1128+6104A	11:28:43.9	61:04:07	0.1452	43516	56	JH	
1128+6100	11:28:56.1	61:00:11	0.1350	40460	300	PH	
1129+6104B	11:29:01.3	61:04:32	0.1410	42260	300	PH	JH
A1287							
1128+6706	11:28:26.0	67:06:02	0.1457	43668	37	JH	
1128+6705	11:28:56.0	67:05:12	0.1408	42205	58	JH	
A1289/8							
1128+6103	11:28:39.2	61:03:18	0.1115	33426	44	JH	
1128+6104	11:28:55.5	61:04:54	0.1119	33545	48	JH	
1128+6059	11:28:56.1	60:59:17	0.1109	33246	48	JH	
A1297							
1130+7632	11:30:33.0	76:32:20	0.1242	37230	47	JH	
1130+7630A	11:30:39.0	76:30:42	0.1253	37572	52	JH	
1130+7630B	11:30:49.0	76:30:22	0.0263	7877	36	JH	Foreground
A1301							
1130+7519	11:30:23.0	75:19:31	0.1225	36711	50	JH	
1130+7524	11:30:53.0	75:24:29	0.1211	36308	54	JH	

TABLE 2—*Continued*

Name	α (1950)	δ	Z	V_h	σ		Comments
A1302							
1130+6639A	11:30:21.0	66:39:13	0.1153	34563	50	JH	
1130+6639B	11:30:22.1	66:39:22	0.1148	34416	54	RK	Same as A??
1130+6639C	11:30:29.6	66:39:04	0.1179	35346	60	RK	
A1315							
1132+7213	11:32:47.0	72:13:07	0.1395	41831	46	JH	
1132+7212	11:32:57.0	72:12:58	0.1424	42678	45	JH	
A1322							
1133+6331A	11:33:15.4	63:31:29	0.1075	32228	100	CFH	
1133+6331B	11:33:23.7	63:31:01	0.1109	33235	38	JH	V=33007 CFH
1133+6331C	11:33:32.5	63:31:02	0.1137	34086	100	CFH	
1133+6330	11:33:39.0	63:30:06	0.1119	33552	38	JH	
A1329							
1135+7123A	11:35:38.0	71:23:54	0.0334	10005	30	JH	Foreground
1135+7123B	11:35:58.0	71:23:31	0.1453	43566	85	JH	
A1331							
1135+6351A	11:35:42.0	63:51:16	0.2046	61337	187	JH	
1135+6351B	11:35:56.0	63:51:08	0.2116	63448	191	JH	
1135+6349	11:35:58.0	63:49:30	0.2068	62005	219	JH	
1136+6351C	11:36:02.6	63:51:38	0.2039	61140	300	PH	
1136+6351D	11:36:06.3	63:51:46	0.1929	57840	300	PH	
1136+6351E	11:36:07.0	63:51:24	0.2139	64132	222	JH	
1136+6350	11:36:02.0	63:50:12	0.2084	62473	233	JH	
1136+6351F	11:36:12.4	63:51:59	0.2159	64735	300	PH	
A1335							
1137+6827	11:37:11.0	68:27: 9	0.1500	44955	42	JH	
A1339							
1138+7320	11:38:51.5	73:20:39	0.1556	46639	55	JH	
A1343							
1138+6054	11:38:08.6	60:54:53	0.1336	40052	100	CFH	
1138+6058	11:38:25.9	60:58:20	0.1291	38698	55	JH	V=38973 CFH
1138+6056	11:38:31.0	60:56:39	0.0638	19137	36	JH	Foreground
A1351							
1139+5847	11:39:40.8	58:47:51	0.3079	92310	300	PH	
1139+5848	11:39:42.0	58:48:44	0.3229	96805	300	PH	
1139+5849	11:39:43.5	58:49:21	0.3349	100400	300	PH	
A1357							
1140+6137A	11:40:20.2	61:37:01	0.1710	51250	300	PH	
1140+6136	11:40:25.8	61:36:32	0.1690	50650	300	PH	
1140+6137B	11:40:25.9	61:37:04	0.1720	51550	300	PH	
1140+6134	11:40:30.0	61:34:36	0.1932	57905	60	JH	Seyfert 2
A1359							
1141+6200	11:41:11.0	62:00:27	0.1787	53587	98	JH	
1141+6157	11:41:14.5	61:57:47	0.1784	53494	63	JH	V=53453 CFH
A1366							
1141+6740	11:41:51.0	67:40:56	0.1159	34735	66	JH	
A1381							
1145+7529	11:45:30.0	75:29:33	0.1165	34923	47	JH	
A1382							
1145+7141	11:45:16.1	71:41:02	0.1050	31478	100	HGT	New Coords
1146+7141	11:46:01.7	71:41:13	0.1046	31367	100	HSM	
A1402							
1150+6040A	11:50:01.0	60:40:12	0.1539	46146	52	JH	
1150+6040B	11:50:37.0	60:40:50	0.1058	31708	48	JH	
1150+6041	11:50:38.0	60:41:09	0.1058	31714	49	JH	
A1406							
1150+6810	11:50:25.0	68:10:34	0.1173	35180	52	JH	

TABLE 2—*Continued*

Name	α (1950)	δ	Z	V_h	σ		Comments
A1412							
1153+7341A	11:53:22.0	73:41:38	0.0833	24973	100	HGT	
1153+7341B	11:53:52.1	73:41:10	0.1080	32378	56	JH	
A1415							
1153+5812	11:53:18.9	58:12:17	0.1590	47672	53	JH	
1153+5808	11:53:19.0	58:08:09	0.1538	46103	56	JH	
1153+5811	11:53:20.0	58:11:44	0.1632	48924	52	JH	
A1421							
1155+6816	11:55:36.0	68:16:48	0.1176	35250	38	JH	
1154+6818	11:54:49.0	68:18:22	0.1188	35614	41	JH	
A1432							
1156+6823	11:56:54.5	68:23:03	0.1130	33870	300	PH	
A1446							
1158+5818	11:58:58.0	58:18:40	0.1034	31004	45	JH	
1159+5818	11:59:31.0	58:18:46	0.1028	30808	34	JH	
A1467							
1202+7255	12:02:31.9	72:55:09	0.1040	31175	51	JH	
1202+7256	12:02:42.2	72:56:37	0.1029	30845	58	JH	
1203+7256	12:03:03.2	72:56:04	0.0225	6740	42	JH	Foreground
A1470							
1204+7156	12:04:24.7	71:56:11	0.1904	57091	237	JH	
1204+7155	12:04:26.6	71:55:58	0.1906	57133	265	JH	
1204+7154	12:04:28.5	71:54:25	0.1926	57751	253	JH	
A1477							
1205+6418A	12:05:49.0	64:18:14	0.1104	33101	55	JH	V=32070 PH
1206+6423	12:06:22.0	64:23:22	0.0868	26020	112	JH	
A1484							
1207+7216A	12:07:53.4	72:16:40	0.1260	37761	210	JH	
1207+7216B	12:07:58.8	72:16:28	0.1241	37193	169	JH	
1208+7216	12:08:01.2	72:16:30	0.1161	34813	170	JH	
A1496							
1211+5936	12:11:19.0	59:36:12	0.0957	28689	100	HGT	
A1500							
1211+7440	12:11:30.0	74:40:00	0.0719	21565	47	JH	
1219+7535	12:19:33.5	75:35:15	0.0708	21239	49	JH	
A1501							
1211+6329A	12:11:39.7	63:29:17	0.1310	39260	300	PH	
1211+6329B	12:11:44.4	63:29:59	0.1300	38960	300	PH	
A1507							
N4199A	12:12:25.9	60:10:24	0.0604	18100	43	JH	
N4199B	12:12:29.1	60:10:28	0.0612	18348	30	JH	
1213+6014	12:13:00.0	60:14:00	0.0604	18106	31	JH	
1213+6015A	12:13:12.0	60:15:00	0.0602	18045	33	JH	
1213+6015B	12:13:18.0	60:15:00	0.0590	17674	31	JH	
1214+6010	12:14:24.0	60:10:00	0.0446	13356	33	JH	
1214+6013	12:14:42.0	60:13:00	0.0433	12971	55	JH	
1214+6014	12:14:42.0	60:14:00	0.0439	13169	29	JH	
A1513							
1214+7304	12:14:24.0	73:04:59	0.1524	45700	52	JH	
A1518							
1216+6347	12:16:15.0	63:47:06	0.0388	11633	47	JH	Foreground?
1216+6345	12:16:29.0	63:45:52	0.1344	40295	55	JH	
1216+6348	12:16:46.0	63:48:22	0.1080	32369	45	JH	
A1528							
1220+5911	12:20:32.3	59:11:12	0.1520	45555	300	PH	
1220+5910	12:20:44.7	59:10:51	0.1560	46755	300	PH	

TABLE 2—*Continued*

Name	α (1950)	δ	Z	V_h	σ		Comments
A1529							
1221+6130	12:21:12.6	61:32:33	0.2319	69530	300	PH	
A1534							
1222+6148	12:22:04.0	61:48:28	0.0695	20844	50	JH	
1222+6146	12:22:09.0	61:46:13	0.0700	20974	45	JH	
1222+6144	12:22:21.0	61:44:53	0.0700	20996	41	JH	
A1536							
1223+7722	12:23:46.0	77:22:42	0.1291	38692	39	JH	
1223+7729	12:23:59.4	77:29:36	0.1186	35560	41	JH	
A1539							
1223+6249	12:23:46.0	62:49: 1	0.1707	51171	60	JH	
A1544							
1225+6339	12:25:33.0	63:39:39	0.1454	43576	41	JH	
A1546							
1225+6452	12:25:48.5	64:52:03	0.2329	69830	300	PH	
A1557							
1230+6308A	12:30:27.2	63:08:18	0.2099	62940	300	PH	
1230+6308B			0.2099	62940	300	PH	
A1559							
1231+6724A	12:31:02.6	67:24:12	0.1049	31454	59	JH	W comp, SGH
1231+6724B	12:31:03.0	67:24:12	0.1084	32488	120	OWT	E comp
A1561							
1230+6939	12:30:46.7	69:39:49	0.1665	49926	338	JH	
1230+6938	12:30:52.0	69:38:49	0.1119	33540	171	JH	
1231+6939A	12:31:00.1	69:39:59	0.1092	32743	181	JH	
1231+6939B	12:31:05.3	69:39:39	0.1805	54120	175	JH	
1231+6940	12:31:11.4	69:40:10	0.0697	20883	65	JH	
A1566							
1232+6438	12:32:52.4	64:38:17	0.1000	29970	300	PH	
1232+6440	12:32:58.6	64:40:13	0.1000	29970	300	PH	
A1576							
1234+6327	12:34:46.3	63:27:40	0.3019	90510	300	PH	
A1579							
1236+6609	12:36:06.9	66:09:48	0.1999	59940	300	PH	
A1590							
1237+7325	12:37:51.0	73:25:51	0.2249	67419	48	JH	
A1597							
1239+7230	12:39:16.3	72:30:10	0.1096	32861	41	JH	
1240+7230	12:40:13.6	72:30:05	0.0756	22656	58	JH	
A1607							
1240+7622	12:40:21.1	76:22:01	0.1355	40614	60	JH	V=40352+105 RK
A1614							
1243+6955	12:43:55.3	69:55:52	0.2289	68630	300	PH	
A1617							
1245+5928	12:45:19.7	59:28:18	0.1520	45555	300	PH	
A1621							
1246+6259A	12:46:23.7	62:59:05	0.1026	30759	69	RK	
1246+6253	12:46:32.9	62:53:32	0.1060	31781	50	JH	
1246+6257	12:46:33.0	62:57:49	0.1010	30287	48	JH	V=30270 PH
1246+6259B	12:46:40.6	62:59:39	0.1019	30548	51	RK	V=30570 PH
A1636							
1251+6305A	12:51:02.6	63:05:35	0.2389	71630	300	PH	
1251+6305B	12:51:10.0	63:05:36	0.2309	69230	300	PH	
A1640							
1252+6250	12:52:24.1	62:50:24	0.1250	37460	300	PH	

TABLE 2—*Continued*

Name	α (1950)	δ	Z	V_h	σ		Comments
A1646							
1253+6225	12:53:55.0	62:25:01	0.1063	31882	56	JH	
A1655							
1256+6537	12:56:30.2	65:37:40	0.2339	70130	300	PH	
A1674							
1300+6744	13:00:50.0	67:44:46	0.1058	31722	43	JH	V=31457 SGH
1301+6743	13:01:29.0	67:43:59	0.1061	31805	48	JH	
A1678							
1303+6229A	13:03:05.6	62:29:37	0.1730	51850	300	PH	
1303+6229B	13:03:06.0	62:29:02	0.1669	50050	300	PH	
A1681							
1303+7204A	13:03:08.0	72:04:03	0.0914	27392	37	JH	
1303+7208	13:03:13.0	72:08:24	0.0899	26942	48	JH	
1303+7204B	13:03:16.0	72:04:14	0.1688	50610	55	JH	
A1683							
1302+7209	13:02:54.0	72:09:06	0.1335	40034	50	JH	
A1687							
1307+5840A	13:07:50.7	58:40:43	0.1959	58740	300	PH	
1307+5840B	13:07:52.4	58:40:31	0.1939	58140	300	PH	
A1695							
1309+6158	13:09:45.9	61:58:19	0.1969	59040	300	PH	
A1701							
1311+6118	13:11:17.0	61:18:53	0.0433	12991	44	JH	Foreground
1311+6115	13:11:45.0	61:15:36	0.1234	36992	59	JH	
A1704							
1312+6450	13:12:35.7	64:50:28	0.2199	65935	300	PH	
A1705							
1311+7310	13:11:28.6	73:10:53	0.2959	88710	300	PH	
A1707							
1313+5829	13:13:45.6	58:29:31	0.1959	58740	300	PH	
A1713							
1317+5818	13:17: 0.0	58:18:58	0.0987	29575	44	JH	
1317+5820	13:17:22.0	58:20:34	0.1405	42124	47	JH	
A1718							
1317+6706	13:17:42.4	67:06:28	0.3339	100100	300	PH	
A1722							
1318+7020A	13:18:38.4	70:20:21	0.3279	98300	300	PH	
1318+7020B			0.3269	98000	300	PH	
A1731							
1320+5825	13:20:59.0	58:25:40	0.1945	58302	56	JH	
A1741							
1323+7140	13:23:03.8	71:40:04	0.0756	22656	41	JH	V=22780 PH
1323+7145	13:23:12.0	71:45:09	0.0723	21674	35	JH	V=21580 PH
A1744							
1323+5935	13:23:57.0	59:35:30	0.1515	45410	57	JH	
A1756							
1328+6228A	13:28:34.8	62:28:57	0.2409	72230	300	PH	
1328+6228B	13:28:41.3	62:28:25	0.3289	98600	300	PH	
A1764							
1332+6012	13:32:55.0	60:12:00	0.1177	35294	53	JH	
1333+6010	13:33:18.0	60:10:33	0.1157	34690	43	JH	

TABLE 2—*Continued*

Name	α (1950)	δ	Z	V_h	σ		Comments
A1767							
1332+5930	13:32:54.7	59:30:56	0.0704	21119	100	HH+	
1332+5939	13:32:57.7	59:39:06	0.0715	21434	100	HH+	
1333+5917A	13:33:10.5	59:17:07	0.0725	21733	100	HH+	
1333+5929	13:33:23.6	59:29:22	0.0644	19307	100	HH+	
1333+5920	13:33:35.6	59:20:34	0.1188	35620	100	HH+	
1333+5930	13:33:43.7	59:30:32	0.0729	21853	100	HH+	
1333+5917B	13:33:45.4	59:17:16	0.0736	22054	100	HH+	
1333+5922	13:33:53.9	59:22:41	0.0709	21260	100	HH+	
1333+5932	13:33:59.8	59:32:13	0.0658	19730	100	HH+	
1334+5929	13:34:08.3	59:29:17	0.0722	21660	100	HH+	
1334+5934	13:34:17.4	59:34:49	0.0748	22438	100	HH+	
1334+5921	13:34:26.1	59:21:10	0.0662	19849	100	HH+	
1334+5937	13:34:59.2	59:37:38	0.0693	20767	100	HH+	
1335+5931	13:35:05.0	59:31:18	0.0725	21727	100	HH+	
1335+5932	13:35:32.0	59:32:43	0.0646	19358	100	HH+	
1335+5938	13:35:38.3	59:38:20	0.0720	21574	100	HH+	
A1776							
1339+5817	13:39:09.0	58:17:46	0.1322	39620	34	JH	
A1777							
1338+7152	13:38:20.7	71:52:42	0.2154	64562	225	JH	
1338+7153A	13:38:31.6	71:53:05	0.3933	117919	200	JH	
1338+7153B	13:38:38.1	71:53:29	0.2147	64370	286	JH	
A1803							
1346+7104	13:46:06.7	71: 4:34	0.1997	59873	46	JH	
A1811							
1348+7116	13:48:38.3	71:16:00	0.1156	34671	232	JH	
1348+7115A	13:48:38.6	71:15:30	0.1187	35575	135	JH	
1348+7114	13:48:39.8	71:14:57	0.1135	34019	131	JH	
1348+7115B	13:48:53.9	71:15:44	0.2513	75325	487	JH	Poor velocity
1348+7115C	13:48:55.5	71:15:07	0.1170	35076	130	JH	
A1848							
1357+7422	13:57:56.7	74:22:40	0.1974	59180	89	JH	
A1851							
1359+7222	13:59:10.6	72:22:09	0.2143	64239	52	JH	
1359+7221	13:59:24.6	72:21:26	0.1370	41086	57	JH	
1358+7220	13:58:11.0	72:20:53	0.0856	25664	36	JH	
1358+7218	13:58:19.9	72:18:28	0.2164	64862	83	JH	
1358+7223	13:58:11.2	72:23:22	0.2123	63648	52	JH	
A1859							
1401+6007	14:01:13.1	60:07:11	0.0988	29619	100	CFH	Foreground
1404+6020B	14:04:11.0	60:20:47	0.2325	69700	330	JH	
1404+6020C	14:04:11.9	60:20:50	0.2372	71120	308	JH	
1404+6021	14:04:04.8	60:21:17	0.2364	70868	400	JH	
1404+6022	14:04:10.7	60:22:44	0.3349	100390	400	JH	
1404+6020D	14:04:20.3	60:20:39	0.2380	71350	400	JH	
1404+6020A	14:04:06.8	60:20:10	0.2326	69720	350	JH	
A1865							
1404+5854A	14:04:06.5	58:54:29	0.1140	34165	300	PH	V=65172+300 JH
1404+5854B	14:04:08.0	58:54:34	0.2217	66470	400	JH	Poor velocity
1404+5854C	14:04:11.9	58:54:57	0.1280	38360	300	PH	V=63834+400 JH
A1872							
1407+6209	14:07:23.5	62:09:52	0.1320	39560	300	PH	
1407+6215	14:07:34.8	62:15:38	0.1508	45208	100	CFH	
1408+6211	14:08:13.0	62:11:14	0.1464	43886	103	JH	Poor velocity

TABLE 2—*Continued*

Name	α (1950)	δ	Z	V_h	σ		Comments
A1877							
1409+6003	14:09:15.0	60:03:17	0.3042	91200	400	JH	Poor velocity
1409+6005	14:09:15.0	60:05:55	0.1241	37204	100	CFH	Foreground ?
1409+6004A	14:09:16.0	60:04:02	0.2493	74726	300	JH	Poor velocity
1409+6004B	14:09:18.6	60:04:02	0.0728	21815	74	JH	Foreground ?
1409+6004C	14:09:25.0	60:04:43	0.3180	95347	400	JH	Poor velocity
A1879							
1409+6351A	14:09:04.2	63:51:17	0.2049	61440	300	PH	
1409+6351B	14:09:03.5	63:51:17	0.2059	61740	300	PH	
A1884							
1407+6123	14:07:09.1	61:23:07	0.1220	36574	100	CFH	Coords??
1410+6138	14:10:13.5	61:38:56	0.1715	51400	61	JH	
1410+6139	14:10:19.0	61:39:14	0.1221	36593	79	JH	
1410+6137	14:10:30.8	61:37:30	0.1212	36328	69	JH	
A1893							
1412+7434	14:12:03.1	74:34:18	0.2049	61440	300	PH	
1412+7428A	14:12:12.2	74:28:19	0.2903	87036	400	JH	
1412+7435	14:12:13.8	74:35:28	0.2079	62340	300	PH	
1412+7428B	14:12:25.7	74:28:56	0.1139	34135	286	JH	
A1895							
1413+7131	14:13:11.8	71:31:42	0.2249	67430	300	PH	
A1918							
1424+6325A	14:24:06.9	63:25:20	0.1380	41371	100	CFH	
1424+6325B	14:24:07.3	63:25:22	0.1392	41731	100	CFH	
1424+6325C	14:24:08.0	63:25:06	0.1409	42234	300	SGH	Same as B???
1424+6331	14:24:48.0	63:31:00	0.1394	41797	65	DJ	Coords??
A1933							
1428+7022	14:28:18.9	70:22:23	0.2148	64386	270	JH	
1428+7021	14:28:25.5	70:21:27	0.2080	62364	290	JH	Poor velocity
1428+7020	14:28:32.3	70:20:54	0.2127	63760	315	JH	
A1937							
1432+5828	14:32:44.8	58:28:23	0.1382	41431	100	CFH	
1433+5829	14:33:10.5	58:29:36	0.1376	41240	51	JH	
A1966							
1442+5904	14:42:33.5	59:04:00	0.1490	44655	300	PH	
1442+5905	14:42:34.0	59:05:45	0.1510	45255	300	PH	
A1969							
1442+6358	14:42:14.5	63:58:25	0.1294	38781	41	JH	
1443+6357	14:43:02.0	63:57:46	0.2981	89365	95	JH	
A1974							
1443+7502A	14:43:29.5	75:02:52	0.1831	54900	300	JH	
1443+7502B	14:43:34.0	75:02:44	0.1746	52337	220	JH	
1443+7502C	14:43:44.7	75:02:33	0.1761	52801	170	JH	Poor velocity
1443+7502D	14:43:46.9	75:02:36	0.1729	51827	78	JH	
1443+7503	14:43:55.3	75:03:00	0.1777	53260	122	JH	
A1975[a]							
1444+6924	14:44:33.6	69:24:27	0.0911	27311	100	CFH	Foreground
1444+6916	14:44:41.0	69:16:45	0.2228	66789	91	JH	
A1995							
1451+5815A	14:51:35.5	58:15:05	0.3159	94705	300	PH	
1451+5815B	14:51:37.0	58:15:05	0.3199	95905	300	PH	
A2002							
1452+6834	14:52:06.5	68:34:34	0.2109	63240	300	PH	
A2013							
1457+6044	14:57:13.0	60:44:46	0.2429	72830	300	PH	
1457+6045	14:57:13.6	60:45:29	0.2359	70730	300	PH	

[a] See notes to Table 1.

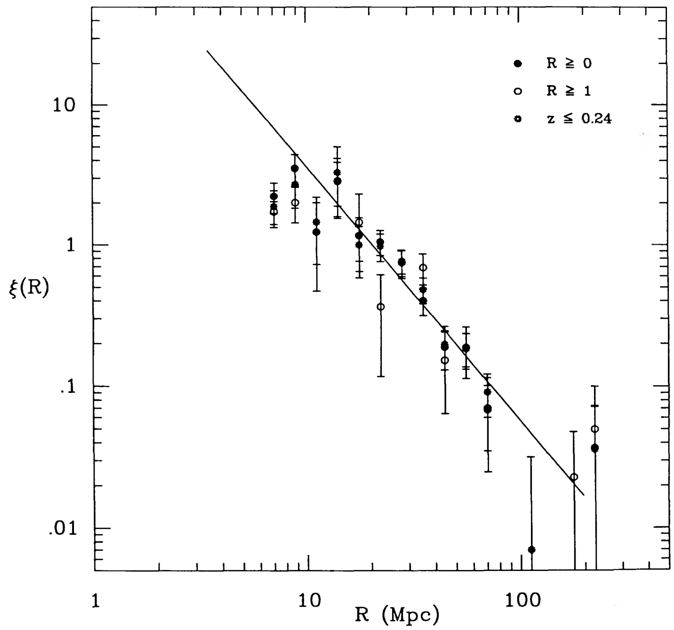

FIG. 4.—Spatial correlation function for deep survey clusters with $R \geq 0$, $R \geq 1$, and $z \leq 0.24$. Bins are logarithmically spaced at intervals of 0.1. Error bars are 1 σ uncertainties. The solid line is the power law $\xi(r) = 230r^{-1.8}$.

samples is substantially larger than in the previous samples because of their smaller size ($\sim$70 clusters).

The amplitude of the spatial correlation function for the $R \geq 1$ deep survey sample is $\sim$1.4 times smaller than that for the $D \leq 4$, $R \geq 1$ sample analyzed by BS [where $\xi(r) \simeq (r/25)^{-1.8}$]. This difference, however, is within the 1 σ uncertainties. The presence of the dense Corona Borealis (CrB) supercluster in the $D \leq 4$ sample is the probable source of the amplitude difference. PGH have demonstrated that the CrB supercluster contributes about 30% of the power in the correlation function for the $D \leq 4$ sample. The deep survey contains no such comparably rich supercluster. If the CrB supercluster is removed from the $D \leq 4$ sample, the spatial correlation length is reduced to $r_0 = 19.6h^{-1}$ Mpc, in even better agreement with the deep survey results. The cluster-cluster correlation lengths derived from the deep survey are also in good agreement with the value of $r_0 = 19.9h^{-1}$ Mpc derived for the volume-limited sample of 152 clusters used by PGH.

It is worth commenting that if we place no constraints on the slope of the correlation function, the best-fit slope for the subsamples studied is -1.5 ± 0.3. If galaxies are largely confined to two-dimensional structures (de Lapparent, Geller, and Huchra 1986; Geller 1987), then the large-scale spatial correlation function will have a slope closer to -1 rather than -2. The physical significance of the flatter slope derived by unconstrained fits to the data, however, will have to await the availability of larger cluster catalogs generated from automated searches.

V. PROJECTION CONTAMINATION

Dekel *et al.* (1988) argue that the $D \leq 4$ Abell cluster sample is seriously affected by "projection contamination." Clusters with small angular separation may have overlapping halos. This overlap may artifically increase the cluster richness. Consequently, a cluster catalog may include systems that would not have satisfied the richness criteria had they been isolated. This type of contamination is a potential problem for any cluster catalog derived by searching for surface density enhancements on the sky. Specifically, Dekel *et al.* find that the amplitude of the spatial correlation function and elongation in the redshift direction are substantially reduced when the $D \leq 4$ sample is "decontaminated." It is important, therefore, to estimate the magnitude of such contamination in our deep survey.

To first order, we know that our sample is not seriously affected by this type of contamination because the correlation lengths are similar for samples with and without $R = 0$ clusters (eqs. [6a] and [6b]). We perform a more rigorous test by simulating the effect of cluster halos. In our simulations, we construct artificial clusters with the projected radial profile

$$\Sigma(r) \propto r^{-1} \quad \text{for } r \leq 1h^{-1} \text{ Mpc}\,, \tag{7a}$$

$$\Sigma(r) \propto r^{-2}; \quad \text{for } r > 1h^{-1} \text{ Mpc}\,. \tag{7b}$$

Note that many cluster profiles fall off faster than r^{-2} for $r > 1h^{-1}$ Mpc (Dressler 1978). In this case our model leads to overestimation of the effect of contamination. In our simulation, we place clusters at the observed positions of the clusters in the real survey and distribute a number of galaxies within an Abell radius which is proportional to the Abell richness class. We assume that galaxies follow a Schechter luminosity function. With the galaxies in place we search within an Abell radius of each cluster center and flag any cluster with a central galaxy count seriously contaminated by interlopers. Such contamination measurements must be done iteratively because the initial cluster richnesses are based on the observed (possibly biased) richnesses. We find, by this technique, that only nine clusters out of the 145 may be seriously contaminated. Of the nine clusters, five are $R = 0$; they would not have been in Abell's catalog had they been more isolated (A1279, A1289, A1432, A1534, A1646). The remaining four clusters are $R = 1$ and would probably have been classified as $R = 0$ if they had been more isolated (A1283, A1640, A1681, A1638). The amplitudes and slopes of the correlation functions for the various subsamples, however, do not change significantly when we exclude these systems from computations. This stability is reassuring and indicates that the correlation function for the deep survey is not seriously biased by projection contamination.

VI. VOID STATISTICS

Observational constraints on the frequency and size of voids in the distribution of galaxies and clusters can place important constraints on theoretical models of galaxy and cluster formation. The statistical significance of voids in the Abell catalog has, however, been a topic of controversy. Bahcall and Soneira (1982) first suggested the presence of a void in the space distribution of a sample of 71 northern Abell clusters in the $D \leq 4$ sample. More recently, Batuski *et al.* (1989) claim to find a void with $75h^{-1}$ Mpc diameter in the Coma/Bootes region. However, Otto *et al.* (1986) and Politzer and Preskill (1986) claim that the *a priori* probability of finding such structures is high enough to make them statistically insignificant.

Our deep survey provides a new probe of the space distribution of Abell clusters. To avoid incompleteness problems, we limit our analysis to the 132 deep survey clusters with $z \leq 0.24$. Figures 5*a* and 5*b* show the redshift distribution of the deep survey clusters with $z \leq 0.24$ as a function of declination. There is a wide region extending from $\sim$40,000 to $\sim$57,000 km s^{-1} in Figure 5*b*, where the cluster density is substantially lower than in the surrounding regions.

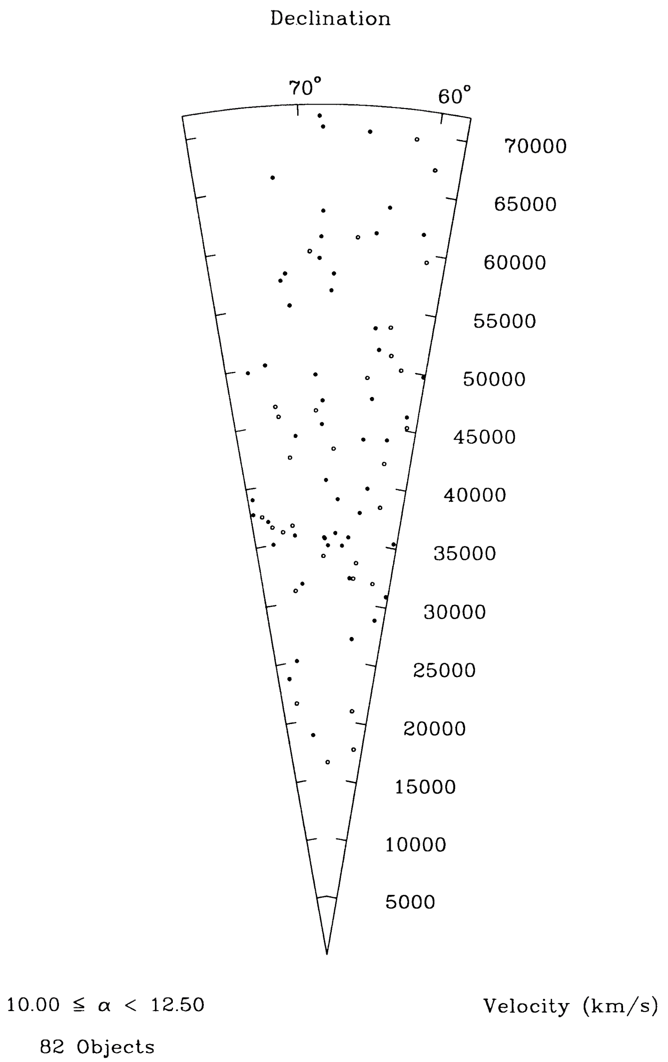

FIG. 5a

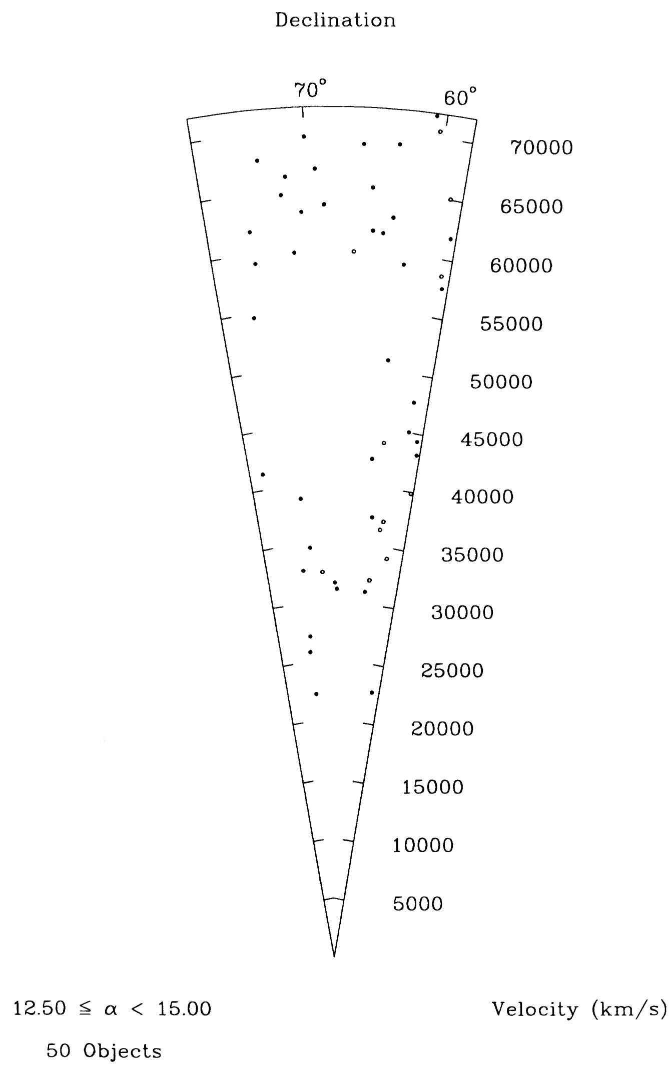

FIG. 5b

FIG. 5.—(*a*) Cone diagram (δ vs. cz) for deep survey clusters with $z \leq 0.24$ and $10^h \leq \alpha < 12^h5$. Open circles represent $R = 0$ clusters; closed circles represent $R \geq 1$ clusters. (*b*) Cone diagram (δ vs. cz) for deep survey clusters with $z \leq 0.24$ and $12^h5 \leq \alpha < 15^h$. Open circles represent $R = 0$ clusters; closed circles represent $R \geq 1$ clusters.

In order to assess the significance of this void, we generate two sets of simulated catalogs. In the first set of simulations, we distribute the clusters randomly. In the second set, the clusters have the same two-point spatial correlation function as the real survey (on scales $< 70h^{-1}$ Mpc). We produce the correlated simulations by placing clusters at the peaks of a Gaussian random phase density field. We adjust the minimum peak density and slope of the power spectrum to match the two-point correlation function of the simulations to the observed deep survey correlation function (eq. [6*c*]). We introduce a short-wavelength cutoff in k-space to remove power on scales greater than $70h^{-1}$ Mpc. Postman *et al.* (1989) give a detailed description of the cluster simulation algorithm.

We generate 50 simulations in each set and include the observed selection effects in redshift and Galactic latitude. We then compute the void probability function (VPF) for the real survey and for the simulations. The VPF is the probability that a randomly selected volume V contains no clusters. For good reviews of the properties of the VPF see White (1979), Schaeffer (1984), Fry (1986), Maurogordato and Lachièze-Rey (1987), and Weinberg, Ostriker, and Dekel (1989).

We compute the VPF by randomly placing 1000 spheres of a given size inside the survey volume, and we count the fraction of those spheres which are empty. We use only spheres which are completely contained within the survey boundaries. We plot the VPF as a function of nV, the mean number of clusters expected within a sphere of volume V in a survey with mean cluster number density n. Figure 6 shows the VPF for the deep survey clusters with $z \leq 0.24$, for the clustered simulations, and for the Poisson simulations. We also plot the relation $P_0(nV) = \exp(-nV)$, the VPF for a Poisson distribution. The results for the simulated catalogs shown in Figure 6 are the mean results for the 50 simulations. The uncertainties are the 1 σ values. The errors for the Poisson simulations are omitted for the sake of clarity but are comparable to the uncertainties for the clustered simulations.

The mean VPF for the clustered simulations agrees very well with the VPF for the deep Abell survey. The VPF for the

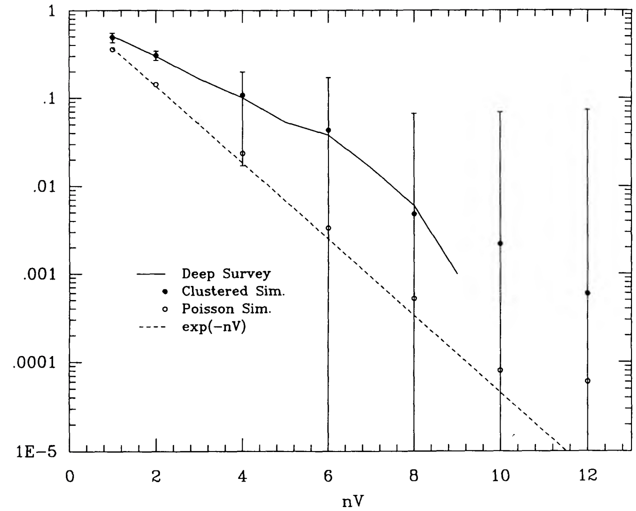

FIG. 6.—Void probability as a function of expected number of clusters in a randomly selected volume. Results are shown for the $z \leq 0.24$ sample of Abell clusters in the deep survey, a series of 50 clustered simulations, and a series of 50 Poisson simulations. The probability for a pure Poisson distribution, $P_0(nV) = \exp(-nV)$, is also shown. Error bars are the 1 σ values.

Poisson simulations is about an order of magnitude smaller than that for the deep survey at $nV = 6$; however the uncertainties are substantial. The VPF for the Poisson simulations is always slightly greater than the expression exp $(-nV)$ primarily because of redshift selection effects. For $nV \geq 10$ (sphere radius $\geq 65h^{-1}$ Mpc), the VPF for the survey is zero. Although the radius of the largest sphere which can be contained within the survey boundaries at $\sim$48,000 km s^{-1} (the mean redshift of the "void") is $\sim 77h^{-1}$ Mpc, the VPF for our survey is consistent with zero for spheres of radius $\gtrsim 65h^{-1}$ Mpc ($nV \geq 10$). To measure the VPF on scales $\gtrsim 70h^{-1}$ Mpc at a statistically significant level (i.e., $nV \gtrsim 12$) requires larger redshift surveys. These results suggest that large voids, like the one in this survey, are relatively common in other deep Abell cluster surveys. The appearance of a large void in this survey is completely consistent with expectations based on the small-scale form and amplitude of the two-point correlation function. We require no power on scales larger than $70h^{-1}$ Mpc, the largest on which the correlation function is significant.

VII. PECULIAR VELOCITIES

Large-scale peculiar velocities are an important issue posed by the analysis of cluster redshift surveys. Bahcall and Soneira (1983) examined the distribution of redshift surveys for cluster pairs in various ranges of angular separation. At small angular separation, they claim a broadening of the redshift distribution caused by relative pairwise peculiar motions of $\sim$2000 km s^{-1} (Bahcall, Soneira, and Burgett 1986). This broadening corresponds to a net elongation of structures along the redshift direction. Correlation function techniques are rigorously valid only when the sample is large enough to average over many systems. In this sample, Soltan (1988) has convincingly demonstrated that the CrB supercluster, which is elongated along the line of sight, substantially enhances the mean amplitude of cluster pair elongations in the redshift direction in the BS cluster sample. It is possible that CrB's elongation reflects the intrinsic geometry of this particular system rather than large-scale peculiar motions (Postman, Geller, and Huchra 1988). When CrB is removed from the sample, no significant deviation from isotropy is found.

We test for elongations by comparing the projected cluster pair separation on the plane of the sky with the separation in the redshift direction. We break the projected separation into two orthogonal components aligned with lines of right ascension (α) and declination (δ) for convenience. When comparing any two components, we require that the third component be $10h^{-1}$ Mpc, or less and that the total spatial separation be $100h^{-1}$ Mpc or less. Because the effective depth of this survey is substantially larger than its projected width, we must exclude all cluster pairs with spatial separations greater than their distances from the survey boundaries. Without this edge correction, we would substantially overestimate the frequency of pairs elongated in the redshift direction. Figure 7*a* shows the histogram for the distribution of pair separations along the redshift and α directions for the 132 $R \geq 0$ deep survey clusters with $z \leq 0.24$. Figure 7*b* shows the histogram for the distribution of pair separations along the redshift and δ directions. The solid histograms show the separations in the α and δ directions after convolution with a Gaussian. The dotted histograms are the unconvolved distributions. The separations in δ are most consistent with the radial separations when convolved with a $\sigma = 900$ km s^{-1} Gaussian. The separations in α are most consistent with the radial separations when convolved with a $\sigma = 700$ km s^{-1} Gaussian. However, the separations in α are consistent with the radial separation distribution even without convolution. The number of pairs decreases as the pair separation increases because of the exclusion of widely separated pairs too near the survey boundaries. Excluding the $R = 0$ clusters from the analysis does not change the results significantly.

Another test for elongation in the redshift direction is the dependence of the angle between the line of sight and the line connecting two clusters (hereafter "the β angle") on the spatial separation of the clusters. If cluster pairs are significantly elongated in the redshift direction (or if there is a Sutherland 1988 style bias in this sample), then clusters with large spatial separation should have a significantly different β-angle distribution than clusters with small spatial separations. Figure 8 shows the histograms of cos β as a function of separation. Again we have excluded pairs too near the survey boundaries. The distributions are all consistent with having been drawn from the same parent population; there is no evidence for substantial elongation in this sample, in agreement with our first test.

For the deep sample, relative peculiar motions are thus $\lesssim$1000 km s^{-1}, inconsistent with the large signal claimed by Bahcall, Soneira, and Burgett (1986). The presence of CrB in the shallow sample is only one of several possible explanations for the difference in results. In deeper samples, it is more difficult to separate close pairs of clusters. If CrB were present in the deep survey, a few of the members might not be identified as separate clusters. Undercounting of these pairs could lead to underestimation of the correlation length and velocity elongation.

VIII. CONCLUSIONS

Our deep cluster is comparable in size to other cluster redshift surveys. The overlap with previous surveys is negligible. The amplitude of the cluster correlation function is a factor of 1.4 smaller than the result originally obtained by Bahcall and Soneira (1983). However, within the large errors, the estimates

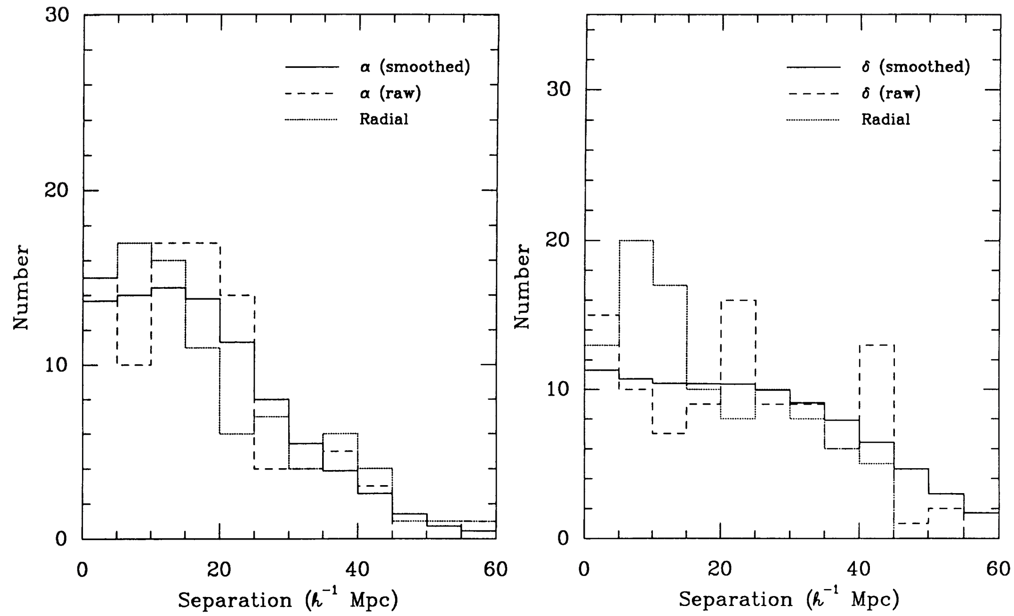

FIG. 7*a* FIG. 7*b*

FIG. 7.—(*a*) Histograms of the distribution of cluster pair separations along the projected (right ascension) and redshift directions. The solid curve represents a convolution of the projected distribution with a 700 km s^{-1} Gaussian. The dotted curve is the unconvolved projected distribution. The redshift distribution is represented by the dashed histogram. (*b*) Same as (*a*), but for projected separations in the declination direction vs. those in the redshift direction. The solid curve represents a convolution of the projected distribution with a 900 km s^{-1} Gaussian.

of the amplitude are consistent. This large amplitude poses a serious problem for attempts to match biased cold dark matter models (White *et al.* 1987) to the data. However, some caution is in order in the evaluation of the discrepancy between the data and the models. The errors in the amplitude of the cluster correlation function are so large that in the $R \geq 1$ and $z \leq 0.24$ subsamples of the deep cluster survey they admit agreement with the amplitude of the galaxy correlation function at the 2 σ level.

In the deep sample there is a large void in the cluster distribution. However, simulations indicate that such voids should be common in a distribution described by the two-point correlation function we derive for the data. No excess power on scales larger than $70h^{-1}$ Mpc is required to explain the void.

This sample puts an upper limit of $\sim$1000 km s^{-1} on peculiar motions. This limit is inconsistent with the previously claimed detection of larger velocities. The discrepancy may

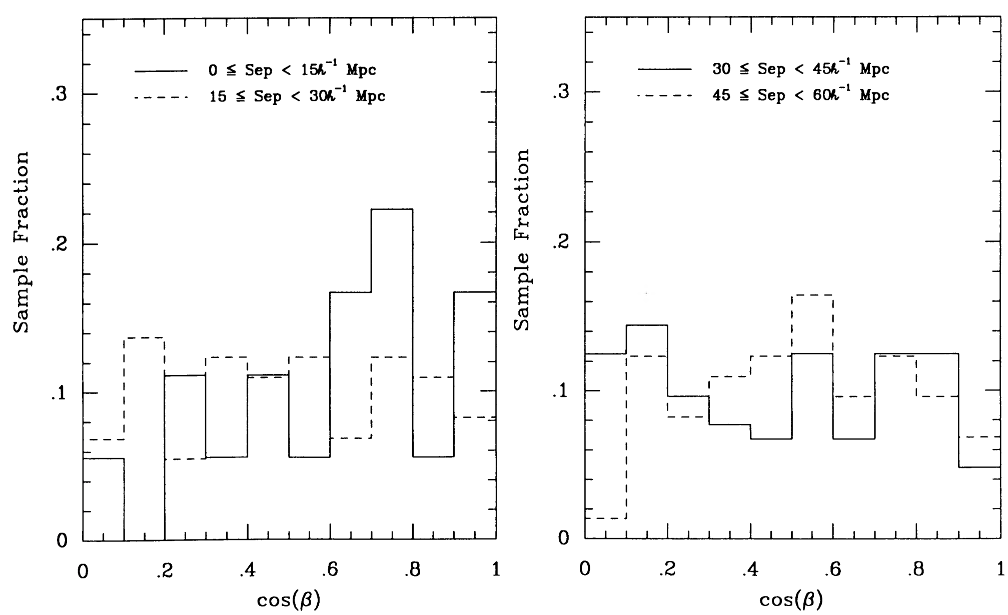

FIG. 8.—Histograms of the cosine of the angle between the line of sight and the line connecting two clusters as a function of cluster pair separation

reflect inadequacies in cluster samples. Large, objectively selected catalogs are necessary to sort out the physics from the observational biases and/or flukes.

We thank John Geary and Kirk Gilmore for helping to make the FOGS work and Robert Hlivak for his work on the IFA CCD systems. We thank the MMT telescope operators, John McAfee, Carol Heller, and Janet Robertson, for able support. Susan Tokarz, Jon Morse, and Gary Hill helped to reduce the data, and Ann Zabludoff measured some of the galaxy positions. We would also like to thank Jaan Einasto for stimulating discussions. This work has been supported in part by the Smithsonian Institution, NASA grant NAGW-201, and NSF grant AST 86-18257 (at Princeton University) and by NSF grant AST 86-15631 (at the University of Hawaii).

REFERENCES

Abell, G. O. 1958, *Ap. J. Suppl.*, **3**, 211.
Bahcall, N. A. 1988, *Ann. Rev. Astr. Ap.*, **26**, 631.
———. 1989, in *Large Scale Motions in the Universe*, ed. Rubin and G. Coyne (Princeton: Princeton University Press), p. 79.
Bahcall, N. A., and Soneira, R. M. 1982, *Ap. J.*, **262**, 419.
———. 1983, *Ap. J.*, **270**, 20 (BS).
Bahcall, N. A., Soneira, R. M., and Burgett, W. S. 1986, *Ap. J.*, **331**, 15.
Batuski, D. J., Burns, J. O., Laubscher, B. E., and Elston, R. J. 1989, preprint.
Ciardullo, R., Ford, H., and Harms, R. 1985, *Ap. J.*, **293**, 69 (CFH).
Davis, M., Peebles, P. J. E. 1983, *Ap. J.*, **267**, 465.
Dekel, A., Blumenthal, G. R., Primack, J. R., and Oliver, S. 1988, *Ap. J. (Letters)*, **338**, L5.
de Lapparent, V., Geller, M. J., and Huchra, J. P. 1986, *Ap. J. (Letters)*, **302**, L1.
———. 1988, *Ap. J.*, **332**, 44.
Dressler, A. 1978. *Ap. J.*, **226**, 55.
Fetisova, T. 1982, *Soviet Astr.* **25**, 647 (F).
Fry, J. N. 1986, *Ap. J.*, **306**, 358.
Geary, J., Huchra, J., and Latham, D. 1986, in *Instrumentation in Astronomy. VI* (*Proc. SPIE*, **627**, 509).
Geller, M. J. 1987, in *Proc. 17th Saas-Fée Course, Large Scale Structure in the Universe*, ed. L. Martinet and M. Mayor (Geneva: Geneva Observatory), p. 69.
Hintzen, P., Hill, J., Lindley, D., Scott, J. S., and Angel, J. R. 1982, *A.J.*, **87**, 1656.
Hintzen, P., Scott, J. S., and McKee, J. D. 1980, *Ap. J.*, **242**, 857.
Hoessel, J. G., Gunn, J. E., and Thuan, T. X. 1980, *Ap. J.*, **241**, 486 (HGT).
Jenner, D. 1974, *Ap. J.*, **191**, 55.
Kirshner, R. P., Oemler, A., and Schechter, P. 1979, *A.J.*, **84**, 493.
Latham, D. 1982, in *IAU Colloquium 67, Instrumentation for Astronomy with Large Optical Telescopes*, ed. C. M. Humphries (Dordrecht: Reidel), p. 259.
Leir, A., and van den Bergh, S. 1977, *Ap. J. Suppl.*, **34**, 381.
Ling, E. N., Frenk, C. S., and Barrow, J. D. 1986, *M.N.R.A.S.*, **223**, 21P.
Lucey, J. R. 1983, *M.N.R.A.S.*, **204**, 33.
Mattig, W. 1958, *Astr. Nach.*, **284**, 109.
Maurogordato, S., and Lachièze-Rey, M. 1987, *Ap. J.*, **320**, 13.
Otto, S., Politzer, H. D., Preskill, J., and Wise, M. B. 1986, *Ap. J.*, **304**, 62.
Owen, F., White, R., and Thronson, H. 1988, *A.J.*, **95**, 1 (OWT).
Palumbo, G., Tanzella-Nitti, G., and Vettolani, G. 1983, *Catalogue of Radial Velocities of Galaxies* (New York: Gordon & Breach).
Peebles, P. J. E. 1980, *The Large-Scale Structure of the Universe* (Princeton: Princeton University Press).
Politzer, H. D., and Preskill, J. P. 1986, *Phys. Rev. Letters*, **56**, 99.
Postman, M., Geller, M. J., and Huchra, J. P. 1986, *A.J.*, **91**, 1267 (PGH).
———. 1988, *A.J.*, **95**, 267.
Postman, M., Spergel, D. N., Sutin, B., and Juszkiewicz, R. 1989, *Ap. J.*, **346**, 588.
Rhee, G., and Katgert, P. 1988, *Astr. Ap. Suppl.*, **72**, 243 (RK).
Sarazin, C., Rood, H., and Struble, M. 1982, *Astr. Ap.*, **108**, L7 (SRS).
Schaeffer, R. 1984, *Astr. Ap.*, **134**, L15.
Schneider, D. 1983, Ph.D. thesis, California Institute for Technology.
Schneider, D., Gunn, J. E., and Hoessel, J. G. 1983, *Ap. J.*, **264**, 337 (SGH).
Shane, C. D., and Wirtanen, 1967, *Pub. Lick Obs.*, Vol. **22**, Part 1.
Shanks, T., Bean, A. J., Efstathiou, G., Ellis, R. S., Fong, R., and Peterson, B. A. 1983, *Ap. J.*, **274**, 529.
Shectman, S. 1985, *Ap. J. Suppl.*, **57**, 77.
Soltan, A. 1988, *M.N.R.A.S.*, **231**, 309.
Sutherland, W. 1988, *M.N.R.A.S.*, **234**, 159.
Tonry, J., and Davis, M. 1979, *A.J.*, **84**, 1511.
Weinberg, D. H., Ostriker, J. P., and Dekel, A. 1989, *Ap. J.*, **336**, 9.
White, S. D. M. 1979, *M.N.R.A.S.*, **186**, 145.
White, S. D. M., Frenk, C. S., Davis, M., and Efstathiou, G. 1987, *Ap. J.*, **313**, 505.

MARGARET GELLER and JOHN HUCHRA: Harvard-Smithsonian Center for Astrophysics, 60 Garden Street, Cambridge, MA 02138

J. PATRICK HENRY: Institute for Astronomy, University of Hawaii, 2680 Woodlawn Drive, Honolulu, HI 96822

MARC POSTMAN: Space Telescope Science Institute, Homewood Campus, Johns Hopkins University, Baltimore, MD 21218